Evaluation of Land Use Land Cover Changes in Nan Province, Thailand, Using Multi-Sensor Satellite Data and Google Earth Engine

Jiratiwan Kruasilp[1,2], Sura Pattanakiat[1*], Thamarat Phutthai[1], Poonperm Vardhanabindu[1], and Pisut Nakmuenwai[1]

[1]Faculty of Environment and Resource Studies, Mahidol University, Nakhon Pathom 73170, Thailand
[2]Geo-informatics and Space Technology Development Agency, Bangkok 10210, Thailand

ARTICLE INFO

Received: 13 Sep 2022
Received in revised: 16 Jan 2023
Accepted: 18 Jan 2023
Published online: 15 Feb 2023
DOI: 10.32526/ennrj/21/202200200

Keywords:
Random forest/ Synthetic Aperture Radar/ Change detection/ Google Earth Engine/ Land management policy

*** Corresponding author:**
E-mail: sura44@gmail.com

ABSTRACT

Land use and land cover (LULC) conversion has become a chronic problem in Nan province. The primary factors of changes are lacking arable land, agricultural practices, and agriculture expansion. This study evaluated the usefulness of multi-sensor Landsat-5 (LS5), Landsat-8 (LS8), Sentinel-1 (S1), and Sentinel-2 (S2) satellite data for monitoring changes in LULC in Nan province, Thailand during a 30-year period (1990-2019), using a random forest (RF) model and the cloud-based Google Earth Engine (GEE) platform. Information of established land management policies was also used to describe the LULC changes. The median composite of the input variables selection from multi-sensor data were used to generate datasets. A total of 36 datasets showed the overall accuracy (OA) ranged from 51.70% to 96.95%. Sentinel-2 satellite images combined with the Modified Soil-Adjusted Vegetation Index (MSAVI) and topographic variables provided the highest OA (96.95%). Combination of optical (i.e., S2 and LS8) and S1 Synthetic Aperture Radar (SAR) data expressed better classification accuracy than individual S1 data. Forest cover decreased continuously during five consecutive periods. Coverage of maize and Pará rubber trees rapidly expanded in 2010-2014. These changes indicate an adverse consequence of the established economic development promoted by industrial and export agriculture. The findings strongly support the use of the RF technique, GEE platform and multi-sensor satellite data to enhance LULC classification accuracy in mountainous area. This study recommended that certain informative and science-based evidence will encourage local policymakers to identify priority areas for land management and natural resource conservation.

1. INTRODUCTION

Land use and land cover (LULC) are changing globally as a result of human activity and land development. In Thailand, LULC changes affect local communities. Accurate, timely, and reliable spatial and temporal information on LULC in mountain areas is crucial, but the information are still lacking. Thailand is often under heavy cloud cover and experiences frequent precipitation. Such weather conditions can affect utilization of optical satellite data in LULC monitoring by reducing image quality. In addition, the optical satellite data sets such as LANDSAT, Satellite Pour l'Observation de la Terre (SPOT), or Moderate Resolution Imaging Spectroradiometer (MODIS) contain limitations. As data acquisitions over the country could be accomplished only a few days per year. Taken together, timely LULC analysis is limited when the single optical sensor data is used.

There has been increasing interest in synthetic aperture radar (SAR) remote sensing, which is sensitive to vegetation structure and can be applied under all weather and environmental conditions (Dobson et al., 1992). However, SAR data has not been widely used for LULC monitoring in Thailand due to the difficulty of image processing operation when compared with optical sensor data. Increasing understanding of the utility of SAR images helps

Citation: Kruasilp J, Pattanakiat S, Phutthai T, Vardhanabindu P, Nakmuenwai P. Evaluation of land use land cover changes in Nan Province, Thailand, using multi-sensor satellite data and Google Earth Engine. Environ. Nat. Resour. J. 2023;21(2):186-197. (https://doi.org/10.32526/ennrj/21/202200200)

driving operational LULC monitoring. Recently, earth observations produce a variety of data across spatial and temporal extents and resolutions. It is desirable to use multi-source data in order to extract LULC information. Therefore, multi-source data can provide superior classification results and fulfill the gaps in data acquisition from single sensor data (Richards, 2012). On the other hand, no study in Thailand has reported the effects of different input variables selecting from multi-sensor satellite data on the accuracy of LULC classification.

Currently, numerous image classification techniques based on remote sensing data were established to improve the accuracy of LULC classification. One of the most robust and generally used techniques of supervised classification techniques for LULC monitoring is Random forest (RF) (Gislason et al., 2006). RF is an ensemble classifier based on bagging to construct many individual decision trees, which is a powerful nonparametric statistical model used to handle non-linear relations. RF is a versatile and smart machine learning technique that can perform both regression and classification tasks using a multitude of decision trees and a statistical technique to produce more accurate and stable predictions (Biau and Scornet, 2016). Compared to other classifiers such as Maximum Likelihood Classification (MLC), Artificial Neural Network (ANN) and Support Vector Machine (SVM), the advantages of RF are processing efficiency on large and multi-source data sets, handling a large number of input variables without variable deletion, and requiring less time for model training (Belgiu and Drăguţ, 2016). Thus, RF is the most frequently used algorithms for satellite image processing over the last 10 years, particularly LULC classification (Rodriguez-Galiano et al., 2012; Balzter et al., 2015; Chakraborty et al., 2016).

To manage multi-sensor datasets at the regional scale, Google Earth Engine (GEE) has been increasingly used in LULC studies in recent years (Amani et al., 2020; Tamiminia et al., 2020). GEE is a free cloud computing platform using JavaScript code for planetary-scale geospatial analyses; it is useful for storing and processing large datasets (Gorelick et al., 2017). GEE provides massive volumes of global time-series satellite images, such as daily MODIS data, Landsat archives dating back to the early 1980s, and Sentinel-1 (S1) and Sentinel-2 (S2) images (Kumar and Mutanga, 2018). Multi-temporal Landsat data were applied to generate LULC maps using machine learning classifier through GEE platform, which showed a consistent and effective overall classification. The result achieved mapping accuracy of greater than 70% (Tsai et al., 2018). In Thailand, GEE is not widely used for operation LULC classification. Therefore, using multi-sensor satellite data and GEE platform is being challenged for robust operational long-term LULC monitoring over the country.

The objective of this study was to evaluate LULC changes in Nan province from 1990 to 2019 using multi-sensor satellite data. A Random forest (RF) classifier was used in conjunction with the GEE platform. Furthermore, the changes in LULC in relation to established land management policies in the province over the last 30 years were revealed.

2. METHODOLOGY

2.1 Study area

The study area is located in Nan province, Thailand (Figure 1), in the easternmost part of Northern Thailand (central coordinates: 100°46' 44.36" E, 18°47'1.61" N), and is bordered by Lao PDR. Nan consists of 15 districts and 99 sub-districts, covering a total area of 12,142.12 km^2. According to the Köppen-Geiger climate map, the region has a tropical savanna climate (Aw) (Peel et al., 2007) with an annual average temperature of around 27°C and average precipitation of around 1,000-1,200 mm per year. The most notable characteristic of the province is its mountain area (87.2%; 600-1,200 meters above mean sea level), which has an average slope of >30%. Nan is flat only in its central valley region, which covers 12.8% of the study area. The dominant forest ecosystems include mixed deciduous forest, evergreen forest, and dry dipterocarp forest. The population of the province was 476,727 in 2020; the main employment sector is agriculture (92.84%) (The Bureau of Registration Administration, 2020).

2.2 Data acquisition

2.2.1 Satellite datasets and topographic variables

This study used multi-sensor satellite data, including S1, S2 MSI S2, Landsat-5 TM (LS5), and Landsat-8 OLI (LS8) images taken over Nan province during 1990 to 2019. These images were selected according to availability on the GEE platform, which covered the study period. The input selected bands of the satellites are given in Table 1. All satellite images were acquired throughout the growing season to

eliminate the influence of seasonal variations in vegetation. In addition, topographic variables consisting of elevation and slope maps were derived from 30-m spatial resolution Shuttle Radar Topography Mission (SRTM) digital elevation models (DEM) based on the WGS84 Geoid model. All datasets were acquired from the US Geological Survey (USGS) website (http://earthexplorer.usgs.gov/) and integrated into the cloud-based GEE platform.

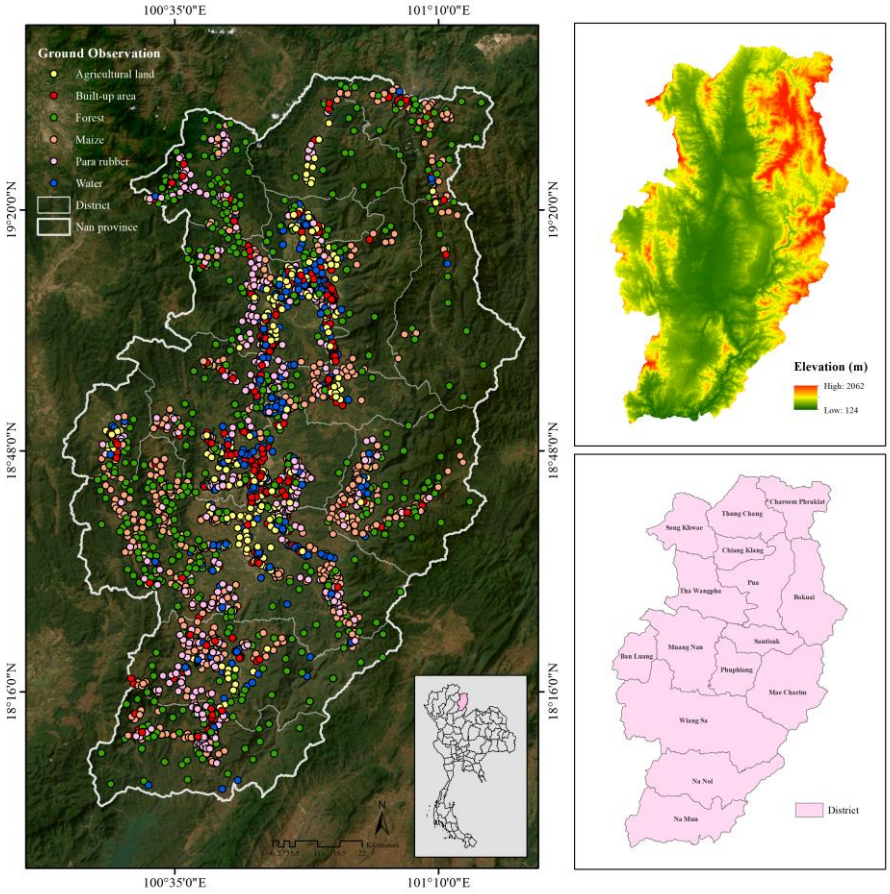

Figure 1. Map of the study area in Nan Province, Thailand. Ground observation map in 2019 (left), elevation map (top right), and administrative boundary map (bottom right).

Table 1. Summary of satellite datasets used in the analysis

Satellite	Data characteristics			
	Sensor	Resolution (m)	Band/Mode	Acquisition
Landsat-5 TM	Optical	30	Visible (band 1 - 3) NIR (band 4) SWIR (band 5)	1990, 1998, 2007, 2010
Landsat-8 OLI	Optical	30	Visible (band 2 - 4) NIR (band 5) SWIR (band 6)	2014, 2019
Sentinel-2 MSI	Optical	10, 20	Visible (band 2 - 4) NIR (band 8) SWIR (band 11)	2019
Sentinel-1 GRD	SAR	10	Dual polarization (VV and VH)	2014, 2019

2.2.1 Ground observations and training data

Ground observation data were collected during the growing season in 2019. In-situ data consisting of digital photographs, longitudes, latitudes, and detailed descriptions of the LULC classes were obtained through ground observations. Six major LULC classes

including agricultural land, built-up area, forest, Pará rubber trees, maize, and water were utilized in this study. Additionally, regions of interest (ROIs) for each LULC class were delineated by visual interpretation of high-resolution Google Earth images, based on advanced knowledge of LULC data acquired through past and ongoing fieldwork (Liu et al., 2018; Sarzynski et al., 2020). Training using an RF classifier and accuracy assessments of LULC maps were conducted using ground observation and ROI data.

2.3 Random forest classification based on Google Earth Engine

2.3.1 Satellite image pre-processing

For optical images pre-processing, LS5, LS8, and S2 surface reflectance images were retrieved from GEE repository. All selected satellite data were calculated for the median image of each study year, which was clipped to the study area boundary. The study area located in the mountain area, where it is subject to cloud cover conditions. Cloud and cloud shadow masking operation using pixel quality assurance band from Landsat surface reflectance images generated from the C programming language implementation of Function of Mask (CFMask) algorithm, was performed to overcome this obstacle (Foga et al., 2017). Meanwhile, the QA60 band was used to mask out clouds from the S2 images. Then, five spectral indices, including the Normalized Difference Vegetation Index (NDVI), Normalized Difference Moisture Index (NDMI), Modified Normalized Difference Water Index (MNDWI), Normalized Difference Built-up Index (NDBI), and Modified Soil-Adjusted Vegetation Index (MSAVI) were calculated from selected images in order to increase the accuracy of LULC classification (Phan et al., 2020). The calculated spectral indices were used as input for LULC classification (Zha et al., 2003; Gitelson, 2004; Xu, 2006; Campbell and Wynne, 2011; DeVries et al., 2015). The specifications of the selected spectral indices are presented in Table 2.

Table 2. Specifications of the spectral indices

Spectral index	Formula
Normalized Difference Vegetation Index	$\frac{\text{NIR} - \text{RED}}{\text{NIR} + \text{RED}}$
Normalized Difference Moisture Index	$\frac{\text{NIR} - \text{SWIR}}{\text{NIR} + \text{SWIR}}$
Modified Normalized Difference Water Index	$\frac{\text{GREEN} - \text{SWIR}}{\text{GREEN} + \text{SWIR}}$
Normalized Difference Built-up Index	$\frac{\text{SWIR} - \text{NIR}}{\text{SWIR} + \text{NIR}}$
Modified Soil-Adjusted Vegetation Index	$\frac{2\text{NIR} + 1 - \sqrt{(2\text{NIR} + 1)^2 - 8(\text{NIR} - \text{RED})}}{2}$

For SAR images pre-processing, S1 Level-1 Ground Range Detected (GRD) images were retrieved from the GEE image library. Orbit restitution, thermal noise removal, terrain correction and radiometric calibration were performed using the Sentinel-1 toolbox on the GEE platform. In addition, S1 images were filtered using refined Lee filter on the GEE platform to reduce speckle noise and preserve content of texture information (Lee et al., 2009). Grey-Level Co-occurrence Matrix (GLCM) is the most popular and approved approach for texture feature extraction. It can improve classification by reducing heterogeneity and preserving boundaries of the same LULC types. The different GLCM texture variables reported in previous studies have increased LULC classification accuracy (Hall-Beyer, 2017; Numbisi et al., 2019; Tavares et al., 2019). In this study, four GLCM texture variables, including variance, contrast, entropy, and correlation, were extracted from backscattering of S1 images. Variance is the dispersion around the average pixel values within a defined window. The depth and smoothness of the image texture structure is reflected by Contrast. Entropy is used to measure the randomness of a gray-level distribution. Correlation is the predictability and linear relationship of the neighboring pixels, which reflects similarity of image texture in a horizontal or vertical direction (Haralick, 1979).

2.3.2 Image classification and LULC change detection using a pixel-based RF classifier

Topographic, optical and SAR products were integrated as features of the classifier input. Each satellite images in 1990, 1998, 2007, 2010, 2014, and

2019 were classified into six major LULC classes including agricultural land, built-up area, forest, para rubber, maize, and water classes. We created six clusters on the GEE platform consisting of (1) LS5/LS8/S1 + spectral indices/GLCM + Topographic variables; (2) LS5/LS8/S1 + spectral indices/GLCM; (3) LS5/LS8/S1; (4) LS5/LS8/S2 + Individual spectral indices + Topographic variables; (5) Combination of LS8/S2 with S1 polarizations + spectral indices + GLCM + Topographic variables; and (6) Combination of LS8/LS2 with S1 polarization. A total of 36 datasets were grouped within six clusters as presented in Table 3. These datasets were selected for evaluation of different input variables selection impact on the accuracy of LULC classification (Phan et al., 2020).

RF supervised machine learning algorithm and GEE platform were utilized to produce LULC maps in 1990, 1998, 2007, 2010, 2014, and 2019. The RF classification was performed using different datasets, including optical spectral bands, five spectral indices, SAR polarizations, four GLCM texture variables for each polarization, and combination of optical and SAR data. Annual cloud free composites of each chosen year were created by using the median reflectance pixel values of the collection (Huang et al., 2010). With a minimum of two tuning parameters requirement, the number of classification trees desired was set at 100 to provide a reliable error estimation and to maintain the computation times. The number of predictor variables used to split a node was set at the square root of the number of input variables (Cutler et al., 2007). All input data were resampled to a resolution of 10 m using a bicubic interpolation to harmonize the different datasets (Vizzari, 2022; De Luca et al., 2022). LULC changes were identified by applying a post-classification comparison method to five consecutive periods: 1990-1998, 1998-2007, 2007-2010, 2010-2014, and 2014-2019 (Tewkesbury et al., 2015).

2.3.3 Accuracy assessment

Accuracy assessment of LULC classification was performed using the confusion matrix, which is accepted as the standard descriptive reporting tool for accuracy assessment (Congalton and Green, 2019). The combination of ground observations and stratified random sampling based on multiple high-resolution Google Earth images were randomly selected to train the RF classifier (70% of pixels from each LULC class) and validate samples (the remaining 30% of pixels) (Belgiu and Drăguţ, 2016). The matrix was used to compute the kappa coefficient (K), overall accuracy (OA), user's accuracy (UA) and producer's accuracy (PA). K is the measurement of RF performance. The possible K values range from -1 (very poor agreement) to 1 (excellent agreement). OA values representing for average percentage of correctly classified pixel range from 0 (no pixel correctly classified) to 1 (100% of pixels are well classified). PA is the measurement of omission error (underestimation) while UA is the measurement of commission error (overestimation).

2.4 Land management policies in Nan Province

Land management policies in Nan Province were collected from governance and online news reports. Thanks to these data, we could confirm results of the LULC changes across the study area for the period 1990-2019. It was found that the forest concession – a policy instrument to implement forest harvesting, promotion of agricultural extension, and infrastructural modernization – resulted in declining of forest from 85% in 1964 to 60% in 2018. To establish an increasing number of protected areas, national parks, and wildlife sanctuaries, the Royal Thai Government officially banned all commercial logging in natural forests in 1989 (Lakanavichian, 2001). This action aimed to encourage projects for maize and Pará rubber plantations in 1981 and 2005, respectively (Thailand Environment Institute, 2012). In the early 21st century, opium was replaced by maize plantation, which was one of the factors of deforestation severity. Rapid booming of maize production resulting in the decline of prices, particularly in 2007. Meanwhile, promoting of Pará rubber plantation occurred as an alternative crop since 2005.

Given all the factors mentioned above, a strategic plan for the province has been promoted to initiate for less adverse environmental impact and increased sustainable consumption of natural resources. It is essential to better understand the sequelae of underlying LULC conversion before effective land use planning. Therefore, the LULC changes would provide the potential information required for design and implementation of natural resources policies, strategies, and legislation. Workflow of the data processing is illustrated in Figure 2.

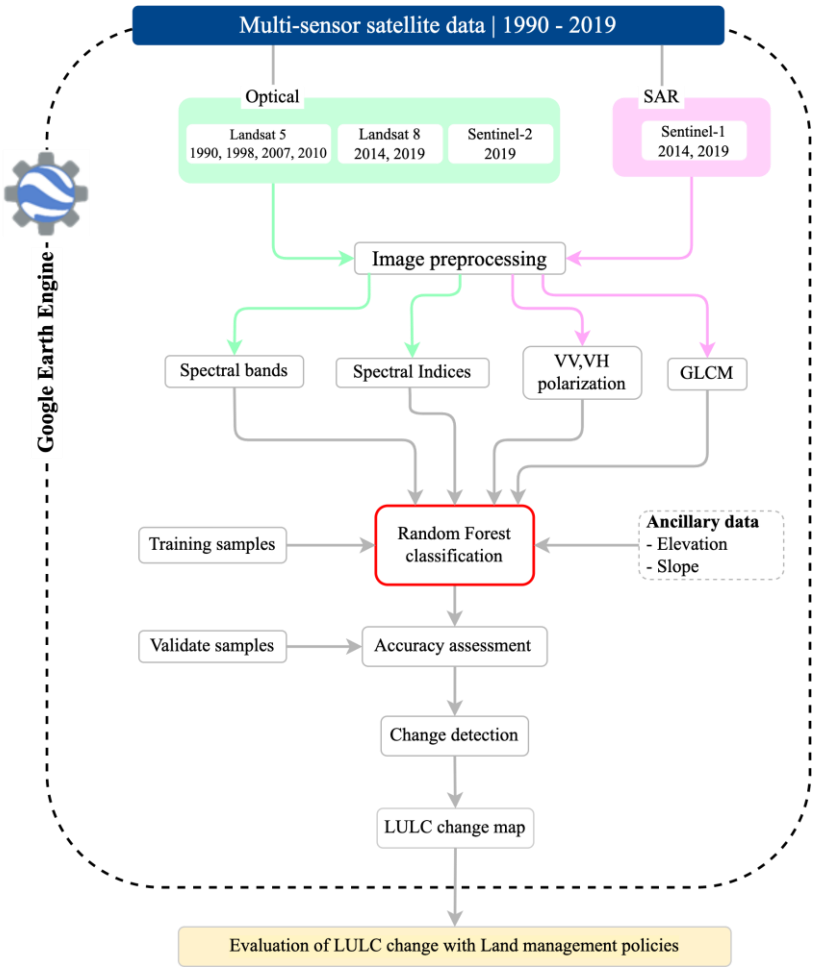

Figure 2. Workflow of data processing

3. RESULTS AND DISCUSSION

3.1 LULC classification based on multi-sensor satellite data using RF via the GEE platform

This study demonstrated the potential of multi-sensor satellite data for monitoring LULC changes in Nan province. In this study, the overall accuracy (OA) of LULC classification for datasets (L01-L36), which were categorized into six clusters, ranged from 51.70% to 96.95% (Table 3). Producer's accuracies (PA) and user's accuracy (UA) values of each dataset ranged from 0.61 to 0.99 and 0.73 to 1, respectively. Dataset L31 in cluster 4 (i.e., S-2 B2, B3, B4, B8, B11, MSAVI, slope, and elevation) provided the highest OA (96.95%; kappa coefficient=0.96), while dataset L15 in cluster 3 (i.e., S1 VV) produced the lowest OA (51.70%; kappa coefficient =0.42). For all clusters, spectral feature bands from LS5, LS8, S2, and a combination of multi-sensor satellite data yielded OA values >85%. This presented high OA compared with previous study using only single sensor (OA<80%) (Phan et al., 2020). Single sensor of optical data was also performed in this study (cluster 3). However, the OA was 85%, which was higher than their study but still lower than OA from multi-sensor. In terms of the SAR data, S1 data alone in clusters 1-3 yielded much lower OA values than LS8, S2, and a combination of multi-sensor satellite data, with an OA <80%. S1 data alone did not provide acceptable classification accuracy in the study area. Possible reasons for this include the low ability of the backscatter intensity feature to identify vegetation, and deep penetration of the C-band into crowns on medium-sized branches (Abdikan et al., 2016). Additionally, similarity between forest backscatter and Pará rubber trees in mountain areas may have decreased the classification accuracy. The results for clusters 5-6 revealed that a combination of multi-sensor satellite images and ancillary variables increased the OA by >12%. Combining optical and SAR satellite images using the RF model resulted in high LULC classification accuracy. This indicated that, compared with utilizing only S2, LS, or S1 data, improvements in classification accuracy could be achieved by combining optical and SAR satellite images. This

result aligned with those of De Alban et al. (2018) and Torbick et al. (2016). Due to their different wavelengths, optical and SAR data respond to different surface characteristics (Zhu et al., 2012). Nevertheless, they provided comparable OA for all LS-8 and S2 spectral bands with the topographic data. However, only the spectral feature bands from S2 images had (slightly) higher OA values than LS8 images. Likewise, combinations of S2 and S1 images provided higher OA than combinations of LS8 and S1 images (cluster 5-6). These findings indicate that the LULC classification results were affected by the spatial resolution of the satellite data obtained by different sensors.

Classification using an RF model and the GEE platform was more accurate than that using maximum likelihood classification (MLC) model in the same study area (Paiboonvorachat and Oyana, 2011). Paiboonvorachat and Oyana (2011) reported OA <86% by using MLC model in Nan province. MLC is a traditional technique, which relies on second order statistics of Gaussian probability density model for each class. The pixel samples are required to have a normal distribution of the data in each class, but some classes are non-normally distributed data. Therefore, this is a significant disadvantage of MLC because input data are regularly non-normal distribution. The GEE platform allows for rapid processing of multi-sensor satellite data, because image downloading and local data storage are not necessary. In contrast, several Thai organizations publishing official national reports of natural resources use conventional techniques for operational image processing, which require expensive hardware and on-premises software.

Table 3. Overall accuracy (%) from the classification results for each datasets

Cluster	Datasets	Variable	OA (%)
1	L1	Landsat-5 B1, B2, B3, B4, B5, NDVI, NDMI, MNDWI, MSAVI, NDBI, slope, elevation	93.65
	L2	Landsat-8 B2, B3, B4, B5, B6, NDVI, NDMI, MNDWI, MSAVI, NDBI, slope, elevation	94.79
	L3	Sentinel-2 B2, B3, B4, B8, B11, NDVI, NDMI, MNDWI, MSAVI, NDBI, slope, elevation	96.42
	L4	Sentinel-1 VV, VV_contrast, VV_var, VV_ent, VV_corr, slope, elevation	70.75
	L5	Sentinel-1 VH, VH_contrast, VH_var, VH_ent, VH_corr, slope, elevation	75.51
	L6	Sentinel-1 VV, VV_contrast, VV_var, VV_ent, VV_corr, VH, VH_contrast, VH_var, VH_ent, VH_corr, slope, elevation	75.21
2	L7	Landsat-5 B1, B2, B3, B4, B5, NDVI, NDMI, MNDWI, MSAVI, NDBI	87.03
	L8	Landsat-8 B2, B3, B4, B5, B6, NDVI, NDMI, MNDWI, MSAVI, NDBI	89.19
	L9	Sentinel-2 B2, B3, B4, B8, B11, NDVI, NDMI, MNDWI, MSAVI, NDBI	91.33
	L10	Sentinel-1 VV, VV_contrast, VV_var, VV_ent, VV_corr	55.10
	L11	Sentinel-1 VH, VH_contrast, VH_var, VH_ent, VH_corr	57.37
3	L12	Landsat-5 B1, B2, B3, B4, B5	85.07
	L13	Landsat-8 B2, B3, B4, B5, B6	89.32
	L14	Sentinel-2 B2, B3, B4, B8, B11	91.23
	L15	Sentinel-1 VV	51.70
	L16	Sentinel-1 VH	58.28
	L17	Sentinel-1 VV, VH	59.64
4	L18	Landsat-5 B1, B2, B3, B4, B5, NDVI, SLOPE, ELEVATION	93.40
	L19	Landsat-5 B1, B2, B3, B4, B5, MSAVI, SLOPE, ELEVATION	93.91
	L20	Landsat-5 B1, B2, B3, B4, B5, MNDWI, SLOPE, ELEVATION	92.39
	L21	Landsat-5 B1, B2, B3, B4, B5, NDBI, SLOPE, ELEVATION	93.65
	L22	Landsat-5 B1, B2, B3, B4, B5, NDMI, SLOPE, ELEVATION	93.40
	L23	Landsat-8 B2, B3, B4, B5, B6, NDVI, slope, elevation	95.33
	L24	Landsat-8 B2, B3, B4, B5, B6, NDMI, slope, elevation	95.06
	L25	Landsat-8 B2, B3, B4, B5, B6, MNDWI, slope, elevation	94.79
	L26	Landsat-8 B2, B3, B4, B5, B6, MSAVI, slope, elevation	95.33
	L27	Landsat-8 B2, B3, B4, B5, B6, NDBI, slope, elevation	94.66
	L28	Sentinel-2 B2, B3, B4, B8, B11, NDVI, slope, elevation	95.54

Table 3. Overall accuracy (%) from the classification results for each datasets (cont.)

Cluster	Datasets	Variable	OA (%)
	L29	Sentinel-2 B2, B3, B4, B8, B11, NDMI, slope, elevation	95.59
	L30	Sentinel-2 B2, B3, B4, B8, B11, MNDWI, slope, elevation	95.74
	L31	Sentinel-2 B2, B3, B4, B8, B11, MSAVI, slope, elevation	96.95
	L32	Sentinel-2 B2, B3, B4, B8, B11, NDBI, slope, elevation	95.33
5	L33	Landsat-8 B2, B3, B4, B5, B6, NDVI, NDMI, MNDWI, MSAVI, NDBI, Sentinel-1 VV, VV_contrast, VV_var, VV_ent, VV_corr, VH, VH_contrast, VH_var, VH_ent, VH_corr, slope, elevation	95.67
	L34	Sentinel-2 B2, B3, B4, B8, B11, NDVI, NDMI, MNDWI, MSAVI, NDBI, Sentinel-1 VV, VV_contrast, VV_var, VV_ent, VV_corr, VH, VH_contrast, VH_var, VH_ent, VH_corr, slope, elevation	96.14
6	L35	Landsat-8 B2, B3, B4, B5, B6, Sentinel-1 VV, VH	91.70
	L36	Sentinel-2 B2, B3, B4, B8, B11, Sentinel-1 VV, VH	92.31

Remarkably, and similar to Mishra et al. (2019), higher OA was obtained in this study by integrating textural features, backscatter intensity, and topographic variables. This was likely due to the texture characteristic, which is an intrinsic spatial feature that effectively represents spatial relationships, particularly in SAR images (Du et al., 2015). The present findings showed that the integration of spectral indices (NDVI, NDMI, MNDWI, MSAVI, and NDBI) from optical sensors and topographic variables (i.e., slope and elevation) can increase LULC classification accuracy. The NDVI is commonly used for efficient classification in tropical forests. Interestingly, the MSAVI enhanced classification accuracy significantly more than the other spectral indices in this study. The loss of forest cover in Nan province has decreased vegetation coverage, but the influence of background soil signals, which are problematic for the NDVI, could be reduced for the MSAVI (Guo et al., 2019; Wen et al., 2020). This result supported the advantage of MSAVI over NDVI which was similar to the finding of Vargas et al. (2021).

Important topographic variables for improving LULC classification accuracy in this study were slope and elevation, because these variables can overcome the similarity of shadow on mountain terrain with the spectral characteristics of waters. This result was supported by previous studies showing that the combination of topographic variables with satellite data provided higher classification accuracy than individual datasets (Wagle et al., 2020; Waśniewski et al., 2020). Likewise, Dobrinić et al. (2021) strongly recommended that topographic variables produced major classification enhancements as an input feature, which was also observed in this study.

3.2 Evaluation of LULC changes by land management policies in Nan province over the last 30 years

The datasets yielding the highest OA values were used to produce LULC maps for 6 study years: 1990, 1998, 2007, 2010, 2014, and 2019 (Figure 3). All LULC classes had producer's accuracies (PA) and user's accuracy (UA) values >0.95. Water was the most differentiable object (PA and UA=0.99 and 1.00, respectively). From 1990 to 2019, the major type of LULC was forest area (70.28%), followed by agricultural area (26.56%). Forest area decreased from 8,533.67 km^2 in 1990 to 7,621.22 km^2 in 2019. Agriculture dominated flat and low-slope areas. A >7-fold increase in maize plantation area was seen between 1990 (159.90 km^2) and 2019 (1,240.87 km^2), whereas the Pará rubber tree area showed a 6.5-fold increase from 2007 to 2019. Slight increases in built-up and water areas were observed, from 1.26% in 1990 to 1.83% in 2019, and 0.58% in 1990 to 0.81% in 2019, respectively.

Over the last three decades (1990-2019), the maize plantation area showed the largest expansion (676.03%), followed by Pará rubber tree (100%) and built-up (45.16%) areas. The smallest expansion, of 39.45%, was that of water area. Agricultural area exhibited the largest decrease, of 22.76%, followed by forest (10.69%) (Figure 4). Across the five consecutive periods, forest was the only area that experienced a continuous decrease, due to its conversion into maize and Pará rubber tree plantation areas. Figure 5 illustrates the forest conversion between 1990 and 2019. Overall forest changed area totally distributed over 1,298.34 km^2. The Pará rubber tree and water areas expanded most between 2007 and 2010 (165.05% and 12.24%, respectively). Maize area expansion was greatest between 1990 and 1998

(256.33%). During the past 30 years, maize and Pará rubber trees have become the dominant monoculture crops in the mountain study area. During that period, both crops were expensive and in high demand on global markets (Pongkijvorasin and Teerasuwannajak, 2019). Their increased cultivation arose from the promotion of industrial and export agriculture by the Thai government and the implementation of a capitalist economic model (Rossi, 2014; Darlington, 2019). The water area was also increased to supply crop plantations. However, the maize plantation area decreased during 2014-2019, by 17.62%, which was related to an increase in the agricultural area. This may be due to the implementation of a strategic plan to grow alternative cash crops to maize, with the aim of reducing adverse effects on the environment.

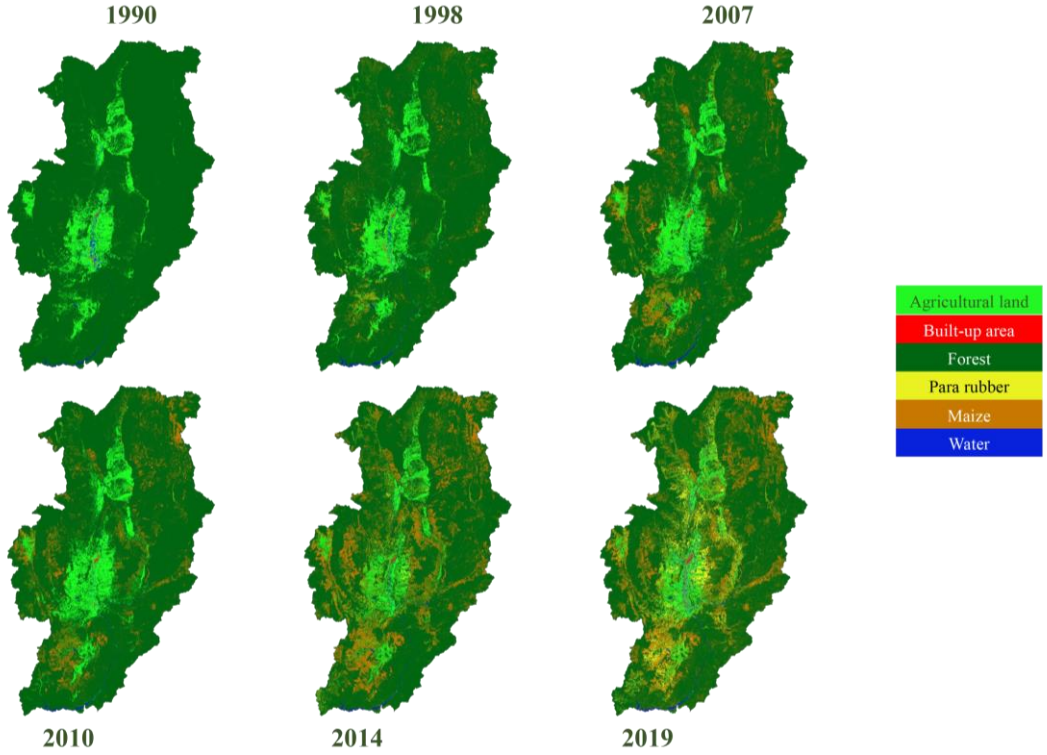

Figure 3. LULC changes between 1990 and 2019 according to the RF classifier

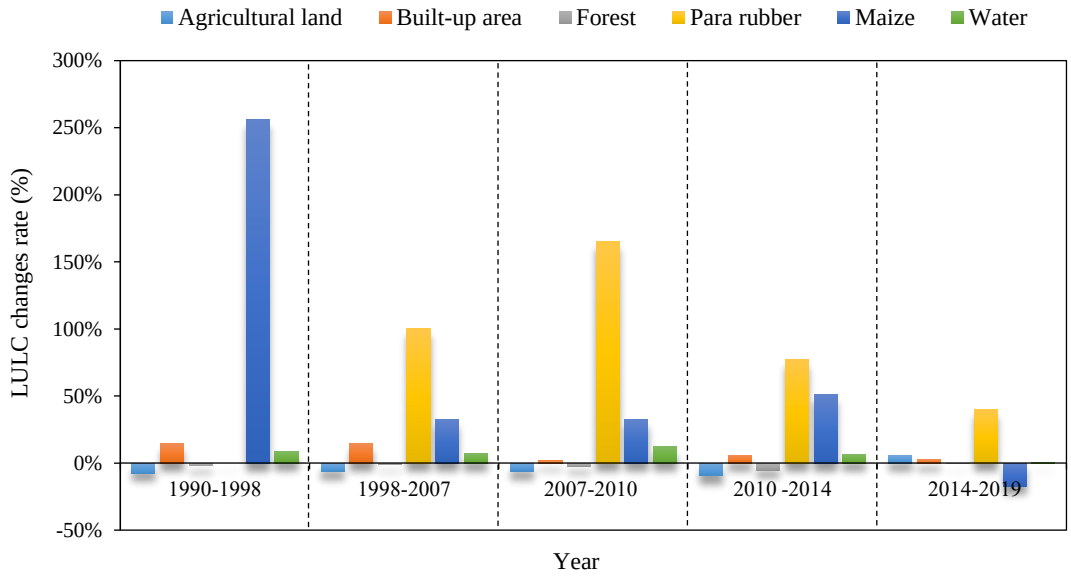

Figure 4. Percentage changes in LULC categories over five consecutive periods

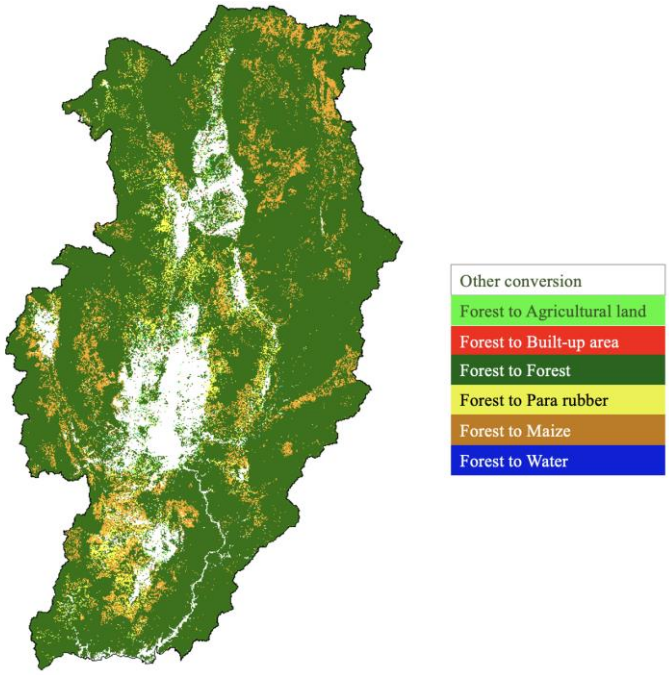

Figure 5. Forest conversion between 1990 and 2019

In the study area, economic measures implemented by the private sector, such as credit provision and market offerings, were among the major drivers of unsustainable land use (Humidtropics, 2015). Forest can be considered as unoccupied land, and there is a lack of awareness of sustainable natural resource use practices. Many farmers transitioned from subsistence farming and small-scale production to cash crops, intensive mono-crop agriculture, and contract farming, as promoted by the government and agro-industrial companies, to generate more income and enhance their quality of life (Darlington, 2019). Even though forest changes are high in Nan province, Agarwal et al. (2022) reported that community managed forests were well conserved due to a strong protection against deforestation by the community. This is a principal key for natural resource management, particularly in forest areas, for sustainable land use and management.

4. CONCLUSION

This study represents the first long-term (30 years) assessment of LULC change in Nan province. Evaluation of the potential of multi-sensor satellite data (i.e., optical and SAR images) to produce LULC change maps in five consecutive periods using an RF model and cloud-computing platform (GEE) was performed. Land management policies were used to clarify the changes of LULC in each period. This study highlighted the advantages of RF classifier in conjunction with GEE platform which can display great performance in rapid processing of multi-sensor satellite data and ability to deal with high-dimensional data. Using GEE platform for LULC change assessment is clearly beneficial for classification purposes and could be used to leverage the operational classification process. The highest overall accuracy was achieved using Sentinel-2 spectral bands, MSAVI, and topographic variables. MSAVI showed an advantage over NDVI in the area of decreased vegetation coverage. Major LULC classification could be enhanced by using topographic variables. In terms of SAR data, the combination of optical (i.e., S2 and LS8) and SAR images expressed better classification accuracy than individual S1 data. Regarding established land management policies, forest areas revealed extensive encroachment in Nan province during the study period. These are consequences of extensive conversion of forest to maize and Pará rubber tree areas. Taken together, geoinformatics and remote sensing technology as well as land management policies will provide certain informed and science-based decisions to guide policymakers in improvement of sustainable natural resource management plan and monitoring.

ACKNOWLEDGEMENTS

The authors would like to thank Geo-Informatics and Space Technology Development Agency (GISTDA), Bangkok, Thailand for supporting

research materials and providing research facilities. We thank the anonymous reviewers and editors for their insightful comments and suggestions.

REFERENCES

Abdikan S, Sanli FB, Ustuner M, Calò F. Land cover mapping using SENTINEL-1 SAR data. Proceedings of the International Archives of the Photogrammetry, Remote Sensing and Spatial Information Sciences, XLI-B7, 2016 XXIII ISPRS Congress; 2016 Jul 12-19; Prague: Czech Republic; 2016.

Agarwal S, Sairorkham B, Sakitram P, Lambin EF. Effectiveness of community forests for forest conservation in Nan Province, Thailand. Journal of Land Use Science 2022;17(1):307-23.

Amani M, Ghorbanian A, Ahmadi SA, Kakooei M, Moghimi A, Mirmazloumi SM, et al. Google earth engine cloud computing platform for remote sensing big data applications: A comprehensive review. IEEE Journal of Selected Topics in Applied Earth Observations and Remote Sensing 2020;13: 5326-50.

Balzter H, Cole B, Thiel C, Schmullius C. Mapping CORINE land cover from Sentinel-1A SAR and SRTM digital elevation kodel data using random forests. Remote Sensing 2015;7(11):14876-98.

Belgiu M, Drăguţ L. Random forest in remote sensing: A review of applications and future directions. ISPRS Journal of Photogrammetry and Remote Sensing 2016;114:24-31.

Biau G, Scornet E. A random forest guided tour. TEST 2016; 25(2):197-227.

Campbell JB, Wynne RH. Introduction to Remote Sensing. New York, USA: Guilford Press; 2011.

Chakraborty A, Sachdeva K, Joshi PK. Mapping long-term land use and land cover change in the central Himalayan region using a tree-based ensemble classification approach. Applied Geography 2016;74:136-50.

Congalton RG, Green K. Assessing the Accuracy of Remotely Sensed Data: Principles and Practices, 3rd ed. Boca Raton, USA: CRC Press; 2019.

Cutler DR, Edwards TC, Beard KH, Cutler A, Hess KT, Gibson J, et al. Random forests for classification in ecology. Ecology 2007;88(11):2783-92.

Darlington SM. Buddhist integration of forest and farm in Northern Thailand. Religions 2019;10(9):Article No. 521.

De Alban JDT, Connette GM, Oswald P, Webb EL. Combined Landsat and L-Band SAR data improves land cover classification and change detection in dynamic tropical landscapes. Remote Sensing 2018;10(2):Article No. 306.

De Luca G, M.N. Silva J, Di Fazio S, Modica G. Integrated use of Sentinel-1 and Sentinel-2 data and open-source machine learning algorithms for land cover mapping in a Mediterranean region. European Journal of Remote Sensing 2022;55(1):52-70.

DeVries B, Decuyper M, Verbesselt J, Zeileis A, Herold M, Joseph S. Tracking disturbance-regrowth dynamics in tropical forests using structural change detection and Landsat time series. Remote Sensing of Environment 2015;169:320-34.

Dobrinić D, Gašparović M, Medak D. Sentinel-1 and 2 Time-Series for vegetation mapping using random forest classification: A case study of Northern Croatia. Remote Sensing 2021;13(12):Article No. 2321.

Dobson MC, Ulaby FT, LeToan T, Beaudoin A, Kasischke ES, Christensen N. Dependence of radar backscatter on coniferous forest biomass. IEEE Transactions on Geoscience and Remote Sensing 1992;30(2):412-5.

Du P, Samat A, Waske B, Liu S, Li Z. Random forest and rotation forest for fully polarized SAR image classification using polarimetric and spatial features. ISPRS Journal of Photogrammetry and Remote Sensing 2015;105:38-53.

Foga S, Scaramuzza PL, Guo S, Zhu Z, Dilley RD, Beckmann T, et al. Cloud detection algorithm comparison and validation for operational Landsat data products. Remote Sensing of Environment 2017;194:379-90.

Gislason PO, Benediktsson JA, Sveinsson JR. Random Forests for land cover classification. Pattern Recognition Letters 2006; 27(4):294-300.

Gitelson AA. Wide dynamic range vegetation index for remote quantification of biophysical characteristics of vegetation. Journal of Plant Physiology 2004;161(2):165-73.

Gorelick N, Hancher M, Dixon M, Ilyushchenko S, Thau D, Moore R. Google Earth Engine: Planetary-scale geospatial analysis for everyone. Remote Sensing of Environment 2017;202:18-27.

Guo B, Yang F, Han B, Fan Y, Chen S, Yang W, et al. A model for the rapid monitoring of soil salinization in the Yellow River Delta using Landsat 8 OLI imagery based on VI-SI feature space. Remote Sensing Letters 2019;10(8):796-805.

Hall-Beyer M. Practical guidelines for choosing GLCM textures to use in landscape classification tasks over a range of moderate spatial scales. International Journal of Remote Sensing 2017;38(5):1312-38.

Haralick RM. Statistical and structural approaches to texture. Proceedings of the IEEE 1979;67(5):786-804.

Huang C, Thomas N, Goward SN, Masek JG, Zhu Z, Townshend JRG, et al. Automated masking of cloud and cloud shadow for forest change analysis using Landsat images. International Journal of Remote Sensing 2010;31(20):5449-64.

Humidtropics. Situational Analysis in Support of the Development of Integrated Agricultural Systems in the Upland Areas of Nan Province, Thailand. Chiang Mai, Thailand: International Institute of Tropical Agriculture; 2015.

Kumar L, Mutanga O. Google Earth Engine applications since inception: Usage, trends, and potential. Remote Sensing 2018;10(10):Article No. 1509.

Lakanavichian S. Forests out of bounds: Impacts and effectiveness of logging bans in natural forests in Asia-Pacific. Bangkok, Thailand: FAO; 2001.

Lee JS, Wen JH, Ainsworth TL, Chen KS, Chen AJ. Improved sigma filter for speckle filtering of SAR imagery. IEEE Transactions on Geoscience and Remote Sensing 2009;47(1): 202-13.

Liu X, Hu G, Chen Y, Li X, Xu X, Li S, et al. High-resolution multi-temporal mapping of global urban land using Landsat images based on the Google Earth Engine Platform. Remote Sensing of Environment 2018;209:227-39.

Mishra VN, Prasad R, Rai PK, Vishwakarma AK, Arora A. Performance evaluation of textural features in improving land use/land cover classification accuracy of heterogeneous landscape using multi-sensor remote sensing data. Earth Science Informatics 2019;12(1):71-86.

Numbisi FN, Van Coillie FMB, De Wulf R. Delineation of cocoa agroforests using multiseason Sentinel-1 SAR images: A low grey level range reduces uncertainties in GLCM texture-based mapping. ISPRS International Journal of Geo-Information 2019;8(4):Article No. 179.

Paiboonvorachat C, Oyana TJ. Land-cover changes and potential impacts on soil erosion in the Nan watershed, Thailand. International Journal of Remote Sensing 2011;32(21): 6587-609.

Peel MC, Finlayson BL, McMahon TA. Updated world map of the Köppen-Geiger climate classification. Hydrology and Earth System Sciences 2007;11(5):1633-44.

Phan TN, Kuch V, Lehnert LW. Land cover classification using Google Earth Engine and random forest classifier: The role of image composition. Remote Sensing 2020;12(15):Article No. 2411.

Pongkijvorasin S, Teerasuwannajak KT. A study of farmer's decision and incentive scheme to reduce highland maize farming in Thailand. International Journal of Agricultural Sustainability 2019;17(3):257-70.

Richards JA. Remote Sensing Digital Image Analysis. Heidelberg, Germany: Springer; 2012.

Rodriguez-Galiano VF, Ghimire B, Rogan J, Chica-Olmo M, Rigol-Sanchez JP. An assessment of the effectiveness of a random forest classifier for land-cover classification. ISPRS Journal of Photogrammetry and Remote Sensing 2012;67:93-104.

Rossi A. Environmental subjects and displays of political order: The case of ecology monks in Northern Thailand. Antropologia 2014;1(1):127-42.

Sarzynski T, Giam X, Carrasco L, Lee JSH. Combining radar and optical imagery to map oil palm plantations in Sumatra, Indonesia, using the Google Earth Engine. Remote Sensing 2020;12(7):Article No. 1220.

Tamiminia H, Salehi B, Mahdianpari M, Quackenbush L, Adeli S, Brisco B. Google Earth Engine for geo-big data applications: A meta-analysis and systematic review. ISPRS Journal of Photogrammetry and Remote Sensing 2020;164:152-70.

Tavares PA, Beltrão NES, Guimarães US, Teodoro AC. Integration of Sentinel-1 and Sentinel-2 for classification and LULC mapping in the urban area of Belém, Eastern Brazilian Amazon. Sensors 2019;19(5):Article No. 1140.

Tewkesbury AP, Comber AJ, Tate NJ, Lamb A, Fisher PF. A critical synthesis of remotely sensed optical image change detection techniques. Remote Sensing of Environment 2015; 160:1-14.

Thailand Environment Institute. Report on the Sub-Global Assessment (SGA) for NAN, Thailand 2012. Thailand: Thailand Environment Institute; 2012. (in Thai).

The Bureau of Registration Administration. Thailand population [Internet]. 2020 [cited 2022 Feb 25]. Available from: https://stat.bora.dopa.go.th/new_stat/webPage/statByYear.php/. (in Thai).

Torbick N, Ledoux L, Salas W, Zhao M. Regional mapping of plantation extent using multisensor imagery. Remote Sensing 2016;8(3):Article No. 236.

Tsai YH, Stow D, Chen HL, Lewison R, An L, Shi L. Mapping vegetation and land use types in Fanjingshan national nature reserve using Google Earth Engine. Remote Sensing 2018;10(6):Article No. 927.

Vargas TF, Vázquez IT, Gómez RA. Remote sensing based forest canopy opening and their spatial representation. Forest Science and Technology 2021;17(4):214-24.

Vizzari M. PlanetScope, Sentinel-2, and Sentinel-1 data integration for object-based land cover classification in Google Earth Engine. Remote Sensing 2022;14(11):Article No. 2628.

Wagle N, Acharya TD, Kolluru V, Huang H, Lee DH. Multi-temporal land cover change mapping using Google Earth Engine and ensemble learning methods. Applied Sciences 2020;10(22):Article No. 8083.

Waśniewski A, Hościło A, Zagajewski B, Moukétou-Tarazewicz D. Assessment of Sentinel-2 Satellite images and random forest classifier for rainforest mapping in Gabon. Forests 2020;11(9):Article No. 941.

Wen Y, Guo B, Zang W, Ge D, Luo W, Zhao H. Desertification detection model in Naiman Banner based on the albedo-modified soil adjusted vegetation index feature space using the Landsat8 OLI images. Geomatics, Natural Hazards and Risk 2020;11(1):544-58.

Xu H. Modification of normalised difference water index (NDWI) to enhance open water features in remotely sensed imagery. International Journal of Remote Sensing 2006;27(14):3025-33.

Zha Y, Gao J, Ni S. Use of normalized difference built-up index in automatically mapping urban areas from TM imagery. International Journal of Remote Sensing 2003;24(3):583-94.

Zhu Z, Woodcock CE, Rogan J, Kellndorfer J. Assessment of spectral, polarimetric, temporal, and spatial dimensions for urban and peri-urban land cover classification using Landsat and SAR data. Remote Sensing of Environment 2012;117:72-82.